ADVANCED MATERIALS

DOI: 10.1002/adma.200703001

Engineering Three-Dimensional Micromirror Arrays by Fiber-Drawing Nanomanufacturing for Solar Energy Conversion**

By *Zeyu Ma, Liyuan Ma,* and *Ming Su**

Efficient light deflection is essential to increase the optical paths of light for a wide range of applications including solar cells[1] and laser-induced desportion–ionization of biomolecules.[2] In the case where multiple deflection units exist, light deflection is closely related to multiple light scattering, which could increase optical absorbance once a light-absorbing material is used. Light scattering has been detected on unpolished silicon after thermal processing, on random textures, on nanoparticle photonic crystals, etc.[3–6] Light deflection, or scattering, has played an important role in improving the efficiencies of thin-film solar cells. However, most methods for making random textured surfaces lack sufficient flexibility and controllability for performance optimization. Another light deflection strategy is dependent on ordered features to control the light path. This strategy uses anisotropic silicon etching to make pyramids and V-shaped grooves in the (100) surface of silicon for light deflection.[7] Microfabricated reflectors could increase the optical paths by more than 10^4 times, where the normal incident light is deflected nearly parallel to the surface.[8,9] In the case of digital micromirror devices, the light path could be adaptively controlled by tilting a micromirror toward or away from a light source.[10] However the lithographic fabrication methods are not ideal for large-scale applications because of the large expense and small size of the surfaces. If a large array of micromirrors can be made in an economic manner, the light absorbance in many engineering areas (i.e., solar cells) could be greatly enhanced.

Fiber-drawing nanomanufacturing (FDN) can make textured surfaces at high yields over large areas with controlled structures and functions. FDN combines scalable fiber-drawing and state-of-the-art differential etching. It offers precise control over the size, aspect ratio, length, and spacing of thus-formed structures of glasses, inorganic materials, and metal alloys.[11–13] Here we describe our efforts in making three-dimensional glass micromirror arrays by combining FDN and differential chemical etching. The cone angle of glass structures can be controlled over the range of 5° to 140° by changing the conditions of chemical etching.

In FDN, a rod of one glass material is inserted into a tube of another glass material to form a preform for fiber drawing (Fig. 1). Both glass materials are selected in such a way that the softening temperatures and coefficients of thermal expansion at the draw temperature are close to each other, but their chemical resistances to an acidic etchant are dissimilar. To make glass micromirror arrays, the tube material is more easily attacked by the etchant than the rod material. The large diameter preform is drawn into a small diameter fiber at high temperature (~880 °). The fiber from the drawing process is cut into short pieces of equal length that are stacked to form a hexagonal bundle for the next drawing. By repeating the same draw-cut-stack cycle, the outer and inner diameters and the wall thickness of the glass tube decrease from centimeters to micrometers while the ordered arrangement of the fibers is preserved. After the second drawing, the fibers are stacked together and annealed around the softening temperature of the glass to make a solid rod. Eventually, the rod is cut perpendicular to its axis to make thin plates that are polished by using different grits and etched in hydrogen fluoride (HF) or a mixture of HF and buffered oxide etchant (BOE) to produce ordered micromirror arrays of glass. The diameter of the glass fibers that can be reliably processed in this method falls between 250 μm and 600 μm. A target diameter of 400 ± 10 μm was chosen because the fiber at this size is relatively strong and has a reasonable size-scaling ratio for the drawing. In a typical experiment, a glass rod with a 22 mm outer diameter and high chemical resistance is put into a glass tube with a 25 mm inner diameter and a 28 mm outer diameter and low chemical resistance. This preform is then drawn into a long fiber with an average diameter of 400 μm at 880 °C and cut to short pieces of 600 mm long. The short pieces are stacked to form a bundle, followed by another draw-cut-stack cycle. Eventually the stacked bundles are annealed at 750 °C to form a rod that will be cut into 1 mm thick plates using a low-speed diamond saw and polished using diamond polishing films with 1 μm and 500 nm powders.

[*] Prof. M. Su, Z. Ma
NanoScience Technology Center
Department of Mechanical, Materials, and Aerospace Engineering
University of Central Florida
Orlando, FL 32826 (USA)
E-mail: mingsu@mail.ucf.edu
Dr. L. Ma
NanoScience Technology Center
University of Central Florida
Orlando, FL 32826 (USA)

[**] We thank Dr. D'Urso at Oak Ridge National Laboratory for guidance in the past years. This project is supported by a New Investigator Research Award from the James and Esther King Biomedical Program of the Florida Department of Health, a Starter G award from the Petroleum Research Fund of the American Chemical Society, a grant from the Florida Space Grant Consortium, and an in-house research grant from the University of Central Florida (UCF).

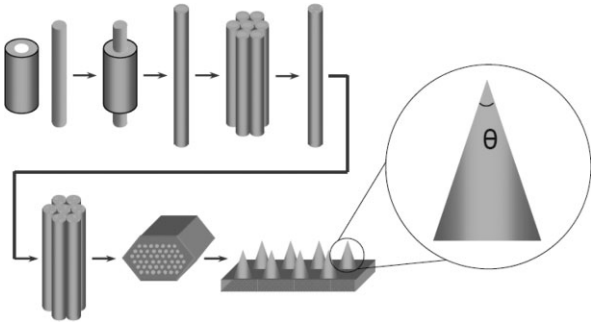

Figure 1. Glass micromirror array made by fiber-drawing nanomanufacturing.

Controlled etching of polished plates creates micromirror arrays on glass. The etching conditions, including the etchant type, etching time, and etchant concentration, determine the final structures. The chemical etching is performed with mild sonication to remove the generated silicon species. The effects of a series of etchants that include 4% by volume HF mixed with 0%, 2.5%, 5%, 10%, and 20% BOE at 20 °C were studied. The BOE buffer keeps the concentration of fluoride ions constant, thus maintaining a nearly constant etching rate. The etching times were varied at 1 min, 5 min, 60 min, 90 min, and 120 min. After etching, the series of samples were rinsed by deionized water, dried in a gentle nitrogen flow, and imaged by using a JEOL 6400 field-emission scanning electron microscope (SEM) after sputtering a thin layer of platinum. Since the two glass materials have different resistance to the etchants, immersing the plate in an etchant creates a topographical contrast on the plates. SEM images indicate ordered glass textures over a large area in different etching solutions and at different times (Fig. 2), where all images were collected with a 30° tilt angle. The distortions in the images of high aspect ratio glasses may be induced by a charging effect, since the sidewalls of these structures are not covered with a uniform layer of platinum. High-resolution imaging has shown facets on some textured structures (Fig. 3a). Figure 3b shows a SEM image of faceted structures collected from the top, where white lines are approximately aligned into a pattern with hexagonal symmetry. The white lines in the images are the result of abundant secondary electrons that escape from the sharp edges of the glass structures (an edge effect). These faceted textures with sharp edges cannot usually be produced in homogenous etching conditions. A possible interpretation is that the adjacent glass cores will affect the local concentrations of etchants due to the spatial restriction. Another possibility is the anisotropic motion of glass melting during the drawing or annealing process.

In contrast to the frequently used anisotropic etching of silicon that makes structures with fixed angles on an opaque substrate, the unique feature of glass micromirrors is that the cone angles depend on the etching conditions in addition to the optical transparency of the glass. This makes the method highly promising for producing glass micromirrors with excellent light deflection properties. Figure 3c shows the effects of etching conditions on the cone angles of glass micromirrors measured from the SEM images. By increasing the volumetric percentage of BOE in the etching solution from 0% to 20%, the cone angle increases from 5° to 140°. The cone angle also increases as the etching time increases. At low BOE concentrations, the cone angle is small due to the large difference in the chemical resistances of the two types of glasses. Increasing the BOE concentration by 2.5% does not significantly change the cone angle, probably because the small amount of fluoride ions does not offer large buffering capability. Increasing BOE concentration from 3% up to 20% increases the cone angles. Additionally, the trends of changes in the cone angles are almost identical when the etching time increases from 30 min to

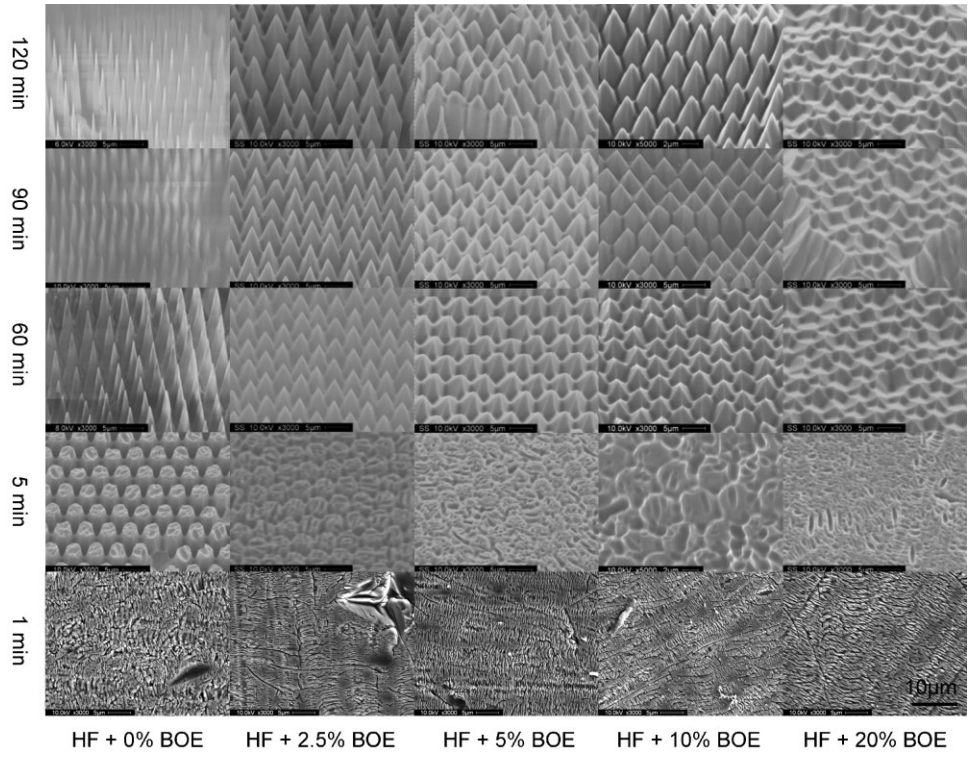

Figure 2. SEM images of etched glass structures obtained under different conditions.

ADVANCED MATERIALS

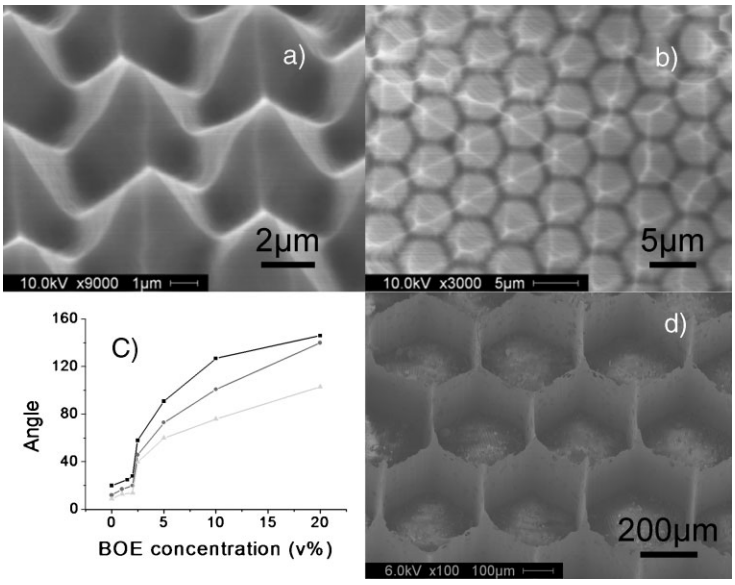

Figure 3. SEM images of facet structures in tilted view (a) and top view (b), the effects of etching conditions on the cone angles measured from SEM images (c), and the differential etching of the glass tube material and the glass core material (d).

120 min. As a comparison, etching the tube material or rod material alone by the same etchant only makes randomized structures on glasses (figures not shown).

The glass tube used in the experiment has more B_2O_3 (16.9%) than the glass rod (13%). The defects created by borate oxides have a larger reactivity with hydrofluoric species to form SiF_4.[14] Assuming the formation and diffusion of SiF_4 into bulk solution is fast, the reaction rates depend on the absorption of fluoride ions on the glass surface, which has been proven as first order, $r = k \cdot C_{HF}$, at low fluoride ion concentrations.[15] At the equilibrium state of the reaction, the cone angle depends on the differential etching rates of the tube and the rod, as well as the diameter of the rod (Fig. 1),

$$\theta = 2\tan^{-1}\left[\frac{d}{2(r_2 - r_1)\cdot t}\right] \quad (1)$$

where r_1 and r_2 are the etching rates of the core glass and the shell glass, respectively, t is the etching time, and d is the diameter of the glass rod. The differential etching rate of the tube material and the rod material was measured using a glass tube to encircle the bundle of fibers from the first drawing. The differential etching rate was determined to be 1.28 μm/min in 4% HF from the 30° tilted SEM image (Fig. 3d). Putting this number into the equation, the cone angle at the etching condition can be calculated as 3.8°, which is close to the value (~5°) measured from the corresponding SEM image.

The transmission spectra of the glass micromirrors were measured by using a Cary 4000 spectrometer, and the reflection spectra were collected on an Ocean Optics mini-spectrometer. For the reflection measurements, a reflection probe, a reflection stage, and a PTFE diffuse reflectance standard were used. A normal incident light (beam size of 2 mm^2) was scattered in all directions by the micromirrors due to multiple reflections. The intensities of transmitted (parallel) and reflected (antiparallel) light were measured as follows. First, the transmission and reflection spectra of a flat glass slide are collected and normalized to 100% in the wavelength range from 400 nm to 900 nm. In order to measure the transmitted light of a micromirror array, one side of a double-sided polished plate is coated with a thin layer of poly(methyl methacrylate) prior to the chemical etching. After etching, the polymer is removed by dipping in dichloromethane, leaving a flat and smooth surface on one side and glass micromirrors on the other. The measured transmission and reflection from a micromirror array show the difference (in percentage) from those of smooth glass slides. The light deflection capability of a micromirror is defined by using the deflection efficiency, DE, i.e., the percentage of deflected light to the light entering the film,

$$DE(\lambda) = \frac{1 - R(\lambda) - T(\lambda)}{R(\lambda) + T(\lambda)} \quad (2)$$

where R and T are measured light reflection and transmission at a certain wavelength. The transmission and reflection spectra of a smooth glass slide are collected as a comparison, which are then subtracted from the according spectra of glass micromirror arrays. The diameter of the glass substrate with the micromirror array is about 4 cm.

Figure 4a shows the wavelength-dependent transmission (curve 1) and reflection (curve 2), and the calculated deflection efficiency (curve 3) of a glass micromirror array obtained by immersing a polished plate in a 2.5% BOE solution for 90 min. The light transmission and reflection of the glass micromirror array at 600 nm is 0% and 2% of the total light intensity, respectively. The transmission data could be less than 0% due to the light intensity fluctuation in the environment. Although in our current setup we cannot measure the distribution of light around the sample, our measurement indicates that more than 98% of the incident light has been deflected by the glass micromirror array. Figure 4b shows the deflection efficiencies of all the glass micromirrors in Figure 2 at a wavelength of 600 nm, where the diameter of each circle is proportional to the magnitude of the deflection efficiency. The deflection efficiencies of glass micromirrors depend on the cone angle and the etching conditions. The maximal DE value is obtained at the cone angle of 60°, which corresponds to an etching time of 120 min in an etchant that has 4% HF and 2.5% BOE. In this case, light entering the structured glass is deflected by the first feature and scattered from one feature to neighboring features. The micromirrors etched in 4% HF for 90 min have almost the same DE value as the one with the maximal DE value. Since the micromirrors obtained under these two conditions have

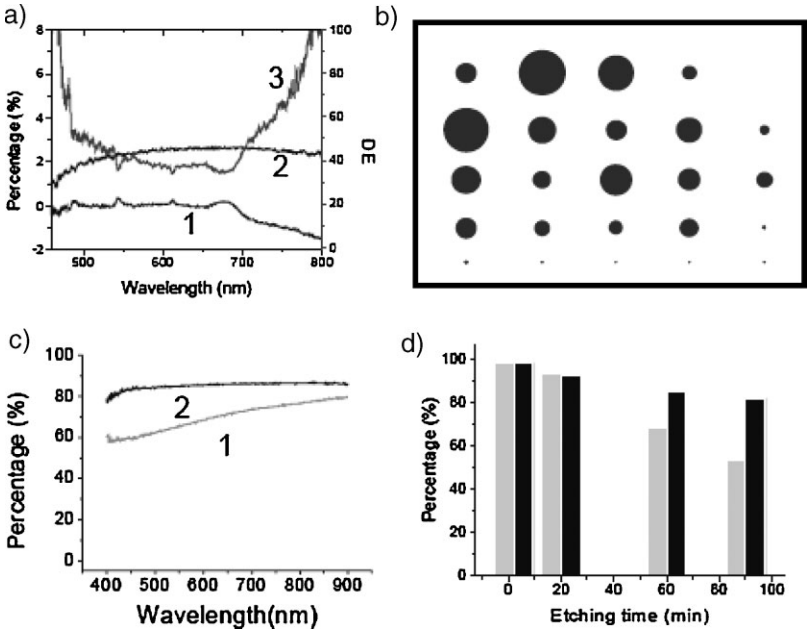

Figure 4. a) Typical transmission, reflection, and *DE* curves of a glass micromirror array. b) Calculated *DE* values of each sample in Figure 2. c) The transmission (curve 1) and the reflection (curve 2) spectra of a glass slide after etching. d) The transmission (gray) and the reflection (black) of glass slides with the same composition as the tube material after etching in HF for 2 min, 20 min, 60 min, and 90 min.

different structures, we conclude that two factors may be important for the light deflection: the cone angle and the height of the glass column. For low aspect ratio micromirrors, the cone angle is more important; for high aspect ratio structures, the height may be more important. In control experiments, we measured both transmission and reflection properties of two glass slides that have the same composition as those of the tube glass and the rod glass, respectively. Figure 4c shows the transmission (curve 1) and reflection (curve 2) spectra of the glass slide that has the same composition as that of the glass tube material after etching for 90 min in a mixture of 4% HF and 5% BOE, where the transmission and reflection values are more than 60%. Longer etching time decreases the light transmission (gray) and reflection (black) of the glass slide significantly in the range of 400 nm to 900 nm (Fig. 4d). These results confirm the effect of glass micromirrors for efficient light deflection.

We used the glass micromirror arrays to make dye-sensitized solar cells. One of the primary factors that limit efficiencies of solar cells is the insufficient absorption of long wavelength photons. For a light-absorbing material with a certain thickness, the light absorbance coefficient drops rapidly as the wavelength increases.[16] According to Beer's law, a long optical path enhances light absorbance. However, thick-film solar cells have low efficiency for electron transport[17] and increased material cost.[18] Even if light absorption efficiency could be high, the overall light–electricity conversion efficiency is low. We coated the micromirror array with a thin film of fluorine-doped tin oxide by chemical vapor deposition as follows.[19] Tin chloride (10 g) and 1 g of ammonium fluoride are dissolved into 120 mL of water. A gentle flow of nitrogen delivers tin chloride into a quartz tube at 600 °C. The tin and fluorine precursors are decomposed in the tube and deposited on a glass micromirror array placed in the center of the tube. The deposition time varies from 0.5 h to 2 h. The composition and structure of the thin film-coated glass were studied by SEM, X-ray diffraction (XRD) and energy dispersive X-ray diffraction (EDX). SEM imaging confirms the presence of the thin film over a large area (Fig. 5a). A high-resolution image shows granular structures on the film (Fig. 5b and 5c). EDX spectra collected at various locations confirm that the surface is covered by tin (Fig. 5d). The lack of a fluorine peak in the figure could be induced by the overlap with the oxygen peak due to the small energy difference of the two elements. The Kα energies of fluorine and oxygen are at 0.7 keV and 0.55 keV, respectively, and thus the two peaks may not be resolved well in the low-energy resolution spectrum. A XRD curve collected

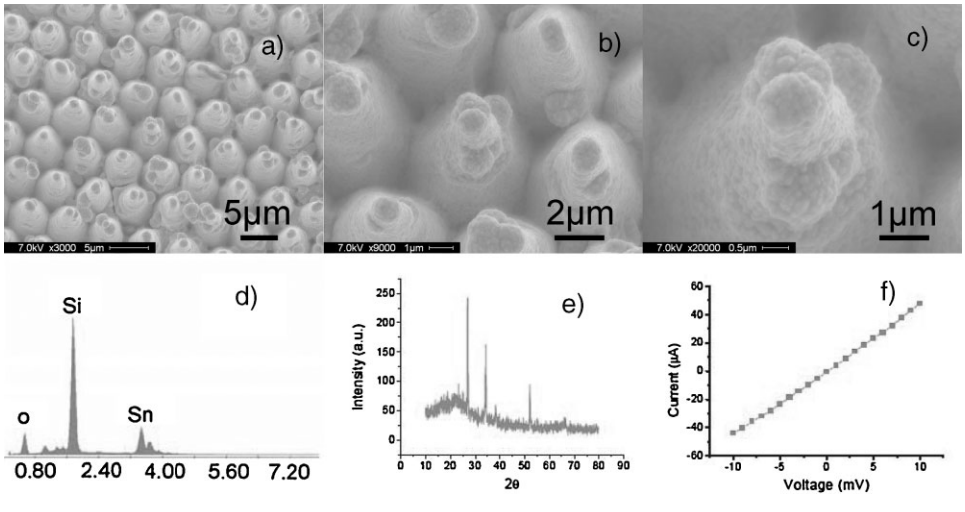

Figure 5. Tin oxide film deposited on glass micromirrors: SEM images (a, b, and c), EDX spectrum (d), XRD curve (e) and current versus voltage curve (f).

ADVANCED MATERIALS

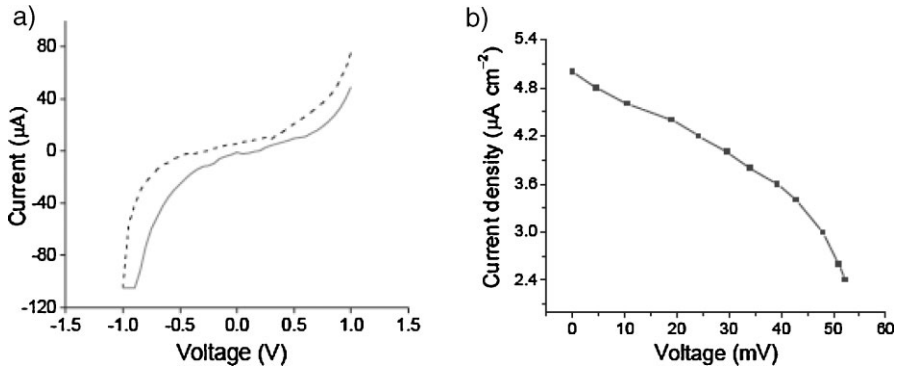

Figure 6. a) Current versus voltage curves collected in dark (dashed) and illuminated (solid) states. b) Current density versus voltage curve at various external loads.

by using CuKα radiation shows that the film has a crystalline tetragonal structure and a preferred orientation along the (110), (101) and (211) planes according to the JCPDS file (Fig. 5e). The formation of the thin film on the surface does not change its light deflection ability. The transmission and reflection are 2% and 1% at 600 nm, respectively. The electric conductivities of the glass micromirrors with tin oxide films were measured by a Keithley 2400 sourcemeter. Figure 5f is the current verses voltage curve of the film, which has a conductivity of 160 Ω cm^{-2}.

We prepared dye-sensitized solar cells on the tin oxide film by coating a thin film of titanium oxide nanoparticles (TiO_2). Briefly, a particle suspension is made by incrementally adding 20 mL of water to 12 g of colloidal TiO_2 powder (Degussa P25). The suspension is then coated on the tin oxide film by spin-coating. The film is allowed to dry in air and then sintered in a furnace at 450 °C for 0.5 h. After slowly cooling down to room temperature, the sample is soaked in 300 μM cis-bis(4,4-dicarboxy-2,2-bipyridine) dithiocyanato ruthenium(II) (N3 Dye) solution for 1 h. The counter electrode is made by coating a carbon thin film on a conductive indium tin oxide (ITO) coated flat glass. The thin carbon film could serve as a catalyst for the oxidation of ions in an electrolyte. In order to assemble a solar cell, the carbon-coated ITO glass is placed on the bottom and the carbon thin film faces up. The dye-stained TiO_2 is placed on the top and the dye-stained TiO_2 side faces the carbon film. The electrolyte is introduced between two electrodes by capillary action. The electrolyte consists of 0.5 M LiI, 0.05 M I_2, and 0.5 M 4-tertbutylpyridine. Active electrode area is around 0.5 cm^2. The measurement was performed by using two digital multimeters under a 75 W incandesce lamp at a distance of 10 cm. Figure 6a shows the current versus voltage curves of the device in the dark or under light. The curve shift indicates the response of the cell, where the dashed line and the solid line correspond to before and after illumination, respectively. We obtained the efficiency curve by changing the external load applied on the solar cell. Figure 6b is the efficiency curve, where the open circuit voltage (V_{oc}) is 55 mV, and the short circuit current density (J_{sc}) is 5 μA cm^{-2}. Since much energy from the lamp is dissipated as heat energy, we do not derive effective efficiency of the solar cell. Further systematical measurements of the efficiencies are planned with rigorous control over the structure of the TiO_2 film and dye-loading, as well as the intensity and distribution of incident light.

Received: December 3, 2007
Revised: June 12, 2008
Published online: September 1, 2008

[1] G. S. Vicente, A. Morales, M. T. Gutierrez, *Thin Solid Films* **2002**, *403*, 335.
[2] S. Okuno, R. Arakawa, K. Okamoto, Y. Matsui, S. Seki, T. Kozawa, S. Tagawa, Y. Wada, *Anal. Chem.* **2005**, *77*, 5364.
[3] A. Usami, *Chem. Phys. Lett.* **1997**, *277*, 105.
[4] L. S. Roman, O. Inganas, T. Granlund, T. Nyberg, M. Svensson, M. R. Andersson, J. C. Hummelen, *Adv. Mater.* **2000**, *12*, 189.
[5] M. J. Stocks, A. J. Carr, A. W. Blakers, *Sol. Energy Mater. Sol. Cells* **1996**, *40*, 33.
[6] J. Zhao, A. Wang, M. A. Green, *Appl. Phys. Lett.* **1998**, *73*, 1991.
[7] H. Ju, P. Zhang, J. Liang, S. Wang, Y. Wu, *J. Micro/Nanolithog. Microfab. Microsys.* **2005**, *4*, 0197011.
[8] S.-S. Lo, C.-C. Chen, F. Garwe, T. Pertch, *J. Phys. D: Appl. Phys.* **2007**, *40*, 754.
[9] L. Zeng, Y. Yi, C. Hong, J. Liu, N. Feng, X. Duan, L. C. Kimerling, B. A. Alamariu, *Appl. Phys. Lett.* **2006**, *89*, 111111.
[10] L. J. Hornbeck, *SPIE Crit. Rev.* **1989**, *1150*, 86.
[11] R. J. Tonucci, B. L. Justus, A. J. Campillo, C. E. Ford, *Science* **1992**, *258*, 783.
[12] B. R. D'Urso, J. T. Simpson, M. Kalyanaraman, *J. Micromech. Microeng.* **2007**, *17*, 717.
[13] X. Zhang, Z. Ma, Z.-Y. Yuan, M. Su, *Adv. Mater.* **2008**, *20*, 1310.
[14] H. Born, M. Prigogine, *J. Chem. Phys.* **1979**, *76*, 538.
[15] H. Kikuyama, M. Waki, M. Miyashita, T. Yabune, N. Miki, J. Takano, T. Ohmi, *J. Electrochem. Soc.* **1994**, *141*, 365.
[16] M. Gratzel, *Nature* **2001**, *414*, 338.
[17] H. J. Snaith, L. Schmidt-Mende, M. Gratzel, M. Chiesa, *Phys. Rev. B: Condens. Matter* **2006**, *74*, 0453061.
[18] A. C. Fisher, L. M. Peter, E. A. Ponomarev, A. B. Walker, K. G. U. Wijayantha, *J. Phys. Chem. B* **2000**, *104*, 949.
[19] T.-H. Fang, W.-J. Chang, *Appl. Surf. Sci.* **2003**, *220*, 175.